Monte Carlo Simulation of the Gas-Phase Volumetric Adsorption System: Effects of Dosing Volume Size, Incremental Dosing Amount, Pore Shape and Size, and Temperature

ARTICLE *in* THE JOURNAL OF PHYSICAL CHEMISTRY B · JUNE 2011

Impact Factor: 3.3 · DOI: 10.1021/jp202073r · Source: PubMed

3 AUTHORS:

Van T Nguyen
University of Queensland
29 PUBLICATIONS **259** CITATIONS
SEE PROFILE

Duong Do
University of Queensland
493 PUBLICATIONS **9,799** CITATIONS
SEE PROFILE

David Nicholson
University of Queensland
294 PUBLICATIONS **4,472** CITATIONS
SEE PROFILE

THE JOURNAL OF PHYSICAL CHEMISTRY B

ARTICLE

pubs.acs.org/JPCB

Monte Carlo Simulation of the Gas-Phase Volumetric Adsorption System: Effects of Dosing Volume Size, Incremental Dosing Amount, Pore Shape and Size, and Temperature

Van T. Nguyen, D. D. Do,* and D. Nicholson

School of Chemical Engineering, University of Queensland, St. Lucia, Qld 4072, Australia

ABSTRACT: We model the volumetric method commonly used in the measurement of gas-phase adsorption isotherms by using Monte Carlo (MC) simulation to study slit pore adsorption in a finite volume. Although the method has been used for a very long time, modeling of the operation by a Monte Carlo scheme to account properly for the exchange of mass between the solid and the finite dosing volume has not been widely studied in the literature. This paper presents the MC simulation of the system composed of the solid subsystem and the gas phase surrounding it. We show that not only the size of the dosing volume and the incremental dosing amount but also the pore shape, pore size, and temperature have significant effects on the unstable region of the phase diagram, especially when the system is going through a first-order transition. This study extends and augments the recent work of Puibasset et al.[1] by showing that the shape of the adsorbent walls and the incremental dosing amount can affect the chemical potential in the adsorption system.

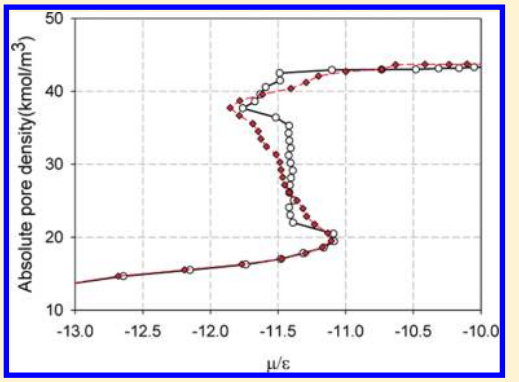

1. INTRODUCTION

Gas-phase adsorption isotherms are commonly obtained with the use of either a volumetric apparatus or a gravimetric method.[2] Between the two, the volumetric method is more popular and more robust than the gravimetric method, and it is no surprise to us that the volumetric method has been adopted by many in their studies of adsorption measurements.[3−10] Basically, the volumetric method involves two volumes: one is the sample volume containing the adsorbent, and the other is the dosing volume. The two are separated by an isolation valve. Initially, the sample volume is evacuated, and the dosing volume is loaded with a known amount of adsorbate which is accurately calculated from an equation of state, $N = f(P,T,V)$. Next, the isolation valve is opened, and the system is allowed to reach equilibrium, at which time the equilibrium pressure is recorded. Traditionally this system is modeled with a grand canonical Monte Carlo scheme in which the adsorbent is exposed to an infinite source of adsorptives at constant chemical potential (which means that mass exchange between the system and the surroundings does not affect the surrounding properties). This model does not exactly reflect the physical process in a volumetric adsorption system because it is in fact a meso-canonical system. The exchange of mass between the adsorbent and the surrounding gas can be modeled by a Monte Carlo (MC) scheme with two simulation boxes. One box represents the porous solid and the other the (adsorptive) gas phase.

Neimark et al.[11−13] have implemented a gauge cell MC simulation method to compute the adsorption isotherms and the gas−liquid equilibrium transition of a Lennard-Jones fluid in cylindrical and spherical pores in which the sample system is connected to a finite reservoir rather than the (effectively) infinite reservoir of the grand ensemble. They demonstrated that the whole van der Waals loop of an adsorption isotherm could be traced in this way in contrast to the single adsorption−desorption transitions found in GCMC. Recently, Puibasset et al.[1] have carried out simulations to study the effects of the size of the gas reservoir on the states visited by a simple fluid (argon at 84 K) adsorbed in a slit nanopore with rectangular carbon dioxide walls with dimension $24\sigma_{ff} \times 8\sigma_{ff}$. Interesting effects were observed in the simulated isotherms which exhibit van der Waals type loops. Here we consider the question of whether the shape of the pore wall has an influence on the unstable states. We also examine the effects of dosing increment, pore size, and temperature on the intermediate states of the adsorption isotherm of the confined fluid. Furthermore, we investigate the 2D-transition in a Lennard-Jones fluid adsorbed on a graphite surface.

2. THEORY

In the MC scheme, we use two simulation boxes and apply the usual Metropolis algorithm to the combined two-box system as a meso-canonical ensemble. Displacement moves are attempted in each box and chosen at random, and attempts to swap particles between the two boxes are carried out to achieve an equalization of chemical potential. A displacement move is accepted with a probability equal to $\min\{1, \exp(-\Delta E/kT)\}$, where ΔE is the

Received: March 4, 2011
Revised: April 20, 2011
Published: May 27, 2011

configuration energy change, and the swap move is accepted with a probability equal to min

$$\left\{1,\ \exp\left(-\frac{\left[\Delta E_{ins}+\Delta E_{rem}+kT\ln\left[\frac{V_{rem}(N_{ins}+1)}{V_{ins}N_{rem}}\right]\right]}{kT}\right)\right\}$$

where ΔE_{ins}, V_{ins}, N_{ins}; ΔE_{rem}, V_{rem}, N_{rem} are the configurational energy change, volume, and number of particles of the "insert" box and the "remove" box, respectively.

The fluid−fluid interaction energy is calculated from the 12-6 Lennard-Jones equation, while the solid−fluid interaction energy is calculated from the Steele 10−4−3 equation. The molecular modeling in this paper is not restricted to these potential equations; it can be used with any potential equations, and it is equally applied to mixtures.

The slit pore is modeled with periodic boundaries in the *x*- and *y*-directions. The cutoff is half the length of the shortest side. The number of cycles was 50 000 for equilibration and for statistics collection. One MC cycle consists of 1000 moves including displacement and attempted particle swaps (equal probability).

The pore density is obtained from simulation as

$$\rho = \frac{\langle N_p \rangle}{V_{acc}} \quad (1)$$

where $<N_p>$ is the ensemble average of the number of particles in the pore volume and V_{acc} is the accessible pore volume. Details of this accessible volume can be found in ref 14.

The chemical potential is contributed by the ideal gas contribution μ_{id} and the excess part μ_{ex}. In this work, we use the Widom insertion method to determine the excess chemical potential of the Lennard-Jones fluid.[15]

$$\mu = \mu_{id}(\rho) + \mu_{ex} = -k_B T \ln\left(\frac{V/\lambda^3}{N+1}\right) - k_B T \ln \int ds_{N+1} \langle \exp(-\beta \Delta U) \rangle_N \quad (2)$$

where λ is the thermal de Broglie wavelength and $< >_N$ denotes canonical ensemble averaging over the configuration space of the *N*-particle system. A coordinate s_{N+1} is generated randomly during simulation, for which we then compute $\exp(-\beta \Delta U)$. By averaging the latter quantity over all generated trial positions, we obtain the average that appears in eq 2.

The pressure can be calculated by the virial equation

$$P = \rho k_B T + \frac{1}{V}\left\langle \sum_{i<j} f(r_{ij}) \cdot r_{ij} \right\rangle \quad (3)$$

where $f(r_{ij})$ is the force between particles *i* and *j* at a distance r_{ij}.

3. RESULTS AND DISCUSSION

3.1. Comparison between the Meso-Canonical Isotherms and GCMC Isotherms. We first illustrate the meso-canonical MC modeling of a volumetric method for argon adsorption at 87.3 K in a 2 nm graphitic slit pore and compare the results with those obtained by a conventional GCMC simulation for the same pore size (Figure 1). This demonstrates that the method can handle capillary condensation and evaporation. The simulation box containing the slit pore has dimensions of 2 × 3.4 × 3.4 nm,

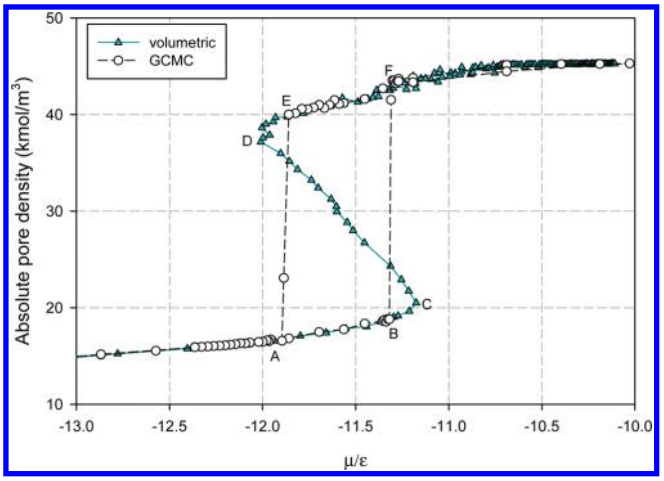

Figure 1. Plot of pore density (based on accessible volume) versus the chemical potential for argon adsorption in the 2 nm graphitic slit pore at 87.3 K with the dosing amount of five particles. The simulation box of the slit pore has dimensions of 2 × 3.4 × 3.4 nm, and the volume of the dosing cell has dimensions of 25 × 25 × 25 nm.

and the dimensions of the dosing cell are 25 × 25 × 25 nm (hereafter we shall denote this size as D25). The ratio of the area dimensions of the adsorbent plane to the pore width is greater than 1.5, which is adequate to model the pore as infinite in extent in the *x*- and *y*-directions.[16]

Initially, these two volumes are free of any adsorbate. The MC simulation is started by inserting a number of particles (dosing increment) into the dosing volume (or gauge cell), and the simulation is carried out in a meso-canonical (*N*, *V*, *T*) ensemble where *V* is the sum of the combined volumes. Once equilibrium is reached, we increase the number of particles in the dosing cell by a small dosing increment. This increment was chosen to be five particles for each equilibrium point (we call the unstable branch an intermediate state). This procedure is repeated until the pore is saturated. The results for the dosing volume D25 are shown in Figure 1 as a plot of the pore density (eq 1) versus the chemical potential of the dosing volume. This isotherm shown as a solid line with triangle symbols in Figure 1 is called the meso-canonical isotherm, which is different from the GCMC isotherm shown as a dashed line with circle symbols. The meso-canonical isotherm exhibits a distinct vdW loop with an unstable branch for which the pore density decreases with the chemical potential, and this is possible with the small size of the dosing volume and the small dosing increment. We will explore the effects of the size of the dosing volume and the size of the increment later.

The adsorption branch of the GCMC isotherm terminates at point B where the fluctuation of the number of particle is such that the interface separating the adsorbed film and the gaseous phase region of the core becomes unstable and the system spontaneously jumps to a liquid-like state, point F. The point of spontaneous condensation in a grand canonical of constant chemical potential (point B) differs from the true stability limit or the vapor-like spinodal, point C, which is reached by the meso-canonical isotherm. The desorption branch of the GCMC isotherm terminates at point E, where the fluid undergoes a spontaneous evaporation prior to the liquid-like spinodal point D of the meso-canonical isotherm. Spontaneous condensation and evaporation occur when the density fluctuations inside the pore are large enough for the system to overcome the free energy

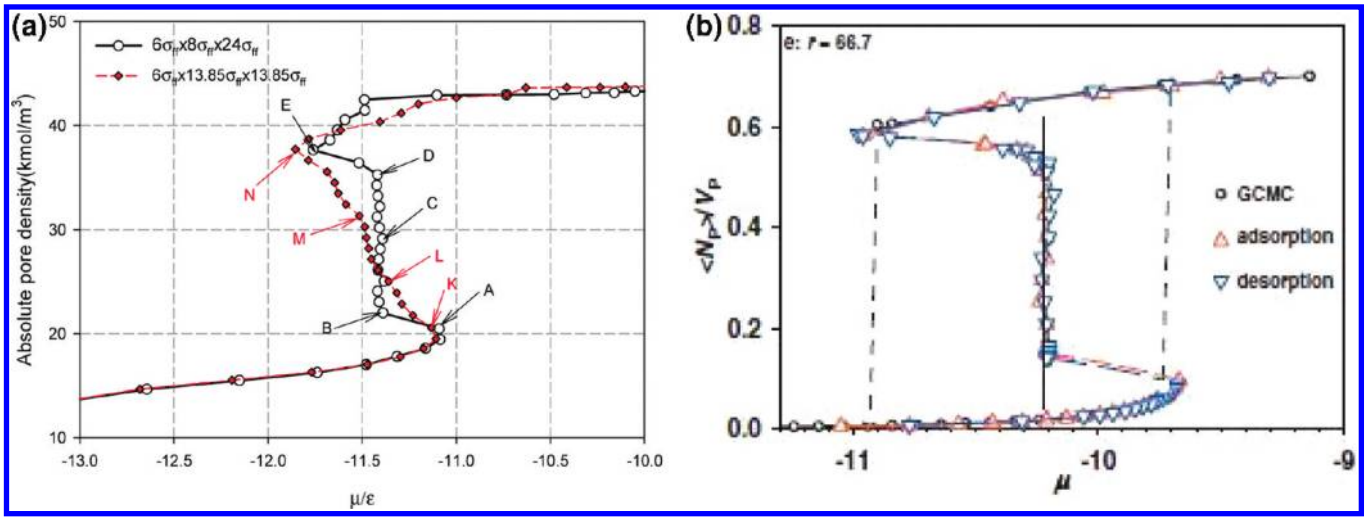

Figure 2. Effects of pore shape on the meso-canonical isotherm of argon adsorption in a $6\sigma_{ff}$ graphitic slit pore. σ_{ff} is the collision diameter of argon (σ_{ff} = 0.3405 nm): (a) at 87.3 K, the ratio of dosing volume to the pore volume is 67. (b) Puibasset data at 83.86 K, the ratio of dosing volume to the pore volume is 66.7.[1]

barrier that separates the phases. As a result these always occur before the respective spinodal limits of stability. However, in the volumetric method for measurement of adsorption, the dosing cell can control the level of fluctuation in the sample cell; therefore, the isotherm can exhibit the entire vdW loop. Between points C and D the fluid can be found in either the vapor or liquid state. From Figure 1 we observe a good agreement between the GCMC isotherm and the meso-canonical isotherm in the region of the stable state, which should be physically expected.

3.2. Effects of the Shape of the Pore Wall. The meso-canonical isotherm in Figure 1 shows a typical vdW loop of S-type behavior. This is observed with a D25 dosing volume, a dosing increment of five particles, and a 2 nm graphitic slit pore whose walls are square in shape. We now investigate the geometry of the pore wall to see how this affects the isotherm. This raises interesting issues which have been previously overlooked in the literature. Instead of using a square wall that leads to the results as shown in Figure 1, we consider a rectangular wall. Puibasset et al.[1] have observed a vertical segment of the intermediate states for argon adsorption at 84 K in a slit nanopore with rectangular walls ($8\sigma_{ff} \times 24\sigma_{ff}$), where σ_{ff} is the collision diameter of argon. Each point on this vertical segment represents a different distribution of particles between the two phases that coexist within the pore.

Figure 2 shows the meso-canonical isotherms for a $6\sigma_{ff}$ graphitic slit pore whose wall dimensions are $8\sigma_{ff} \times 24\sigma_{ff}$ and reproduces the results of Puibasset et al. with a clear vertical segment that represents the coexistence of the two phases within the pore. The ratio of the dosing volume to the pore volume is 67 (compare Figure 1e in ref 1). Also shown in the same figure is the meso-canonical isotherm of the same pore width with a square wall having the same area as that of the rectangular wall. Since periodic boundary conditions are applied in the *x*- and *y*-directions, one would expect that the shape of the pore wall should not have any effects, but to our surprise it does have a significant effect on the intermediate states. For a square wall, we do not observe a vertical segment of the intermediate states. Why does the wall shape have a profound influence on the intermediate states but not on the metastable and stable states? We search for a resolution on this matter by first considering the snapshots of various points as marked in Figure 2. For the points B, C, and D on the vertical segment of the intermediate states of the pore system having rectangular walls, we clearly see the segregation of the two phases, while for points K, L, and M of the pore system having square walls we do not detect any clear segregation (Figure 3). This is due to the symmetry in the *x*- and *y*-directions of the square walls. With the rectangular wall, that symmetry is broken, and as a result two phases can coexist with a liquid bridge forming along the *x*-direction, which is the shorter length of the rectangular wall. This is a consequence of the finite size cell. At point A the particle number is not enough to form a liquid bridge, but rather the particles are confined close to the pore wall. When the number of particles is increased to point B, we see the formation of a liquid bridge, and the increase in density along the vertical segment of the intermediate states is reflected in the displacement of the two interfaces to reduce the vapor bubble in the pore. This process occurs at a constant chemical potential. On the other hand, in the case of a square wall the fluctuation of particles in the *x*- and *y*-directions retains the symmetry, which makes the system more difficult to separate into two phases. This raises the question of whether this symmetry prevents the phase separation when the size of the wall is increased. We shall leave this until Section 3.5.

3.3. Effects of the Dosing Volume on the Behavior of Pores Having Square Walls. Puibasset et al.[1] reported the effects of the size of the dosing volume on argon adsorption at 84 K in a slit nanopore having a rectangular wall ($8\sigma_{ff} \times 24\sigma_{ff}$). We investigate this for argon adsorption at 87.3 K in a 2 nm graphitic slit nanopore having square walls by using the same increment of five particles in each dose but varying the size of the dosing volume. We present in Figure 4 plots of the pore density (based on accessible volume) versus chemical potential for different sizes of the dosing volume.

When we increase the dosing volume size from D25 to D30, we see no change in the meso-canonical isotherm. This means that the unstable branch of this isotherm is dependent on the adsorbent−adsorbate pair (independent of the size of the dosing volume). However, as the size of the dosing volume is increased to D40, D50, and D60, we see a significant change in the meso-canonical isotherm as these sizes are large enough to induce large fluctuations in the pore volume (Figure 5) in a manner that the unstable states of the system could not be isolated, but rather the

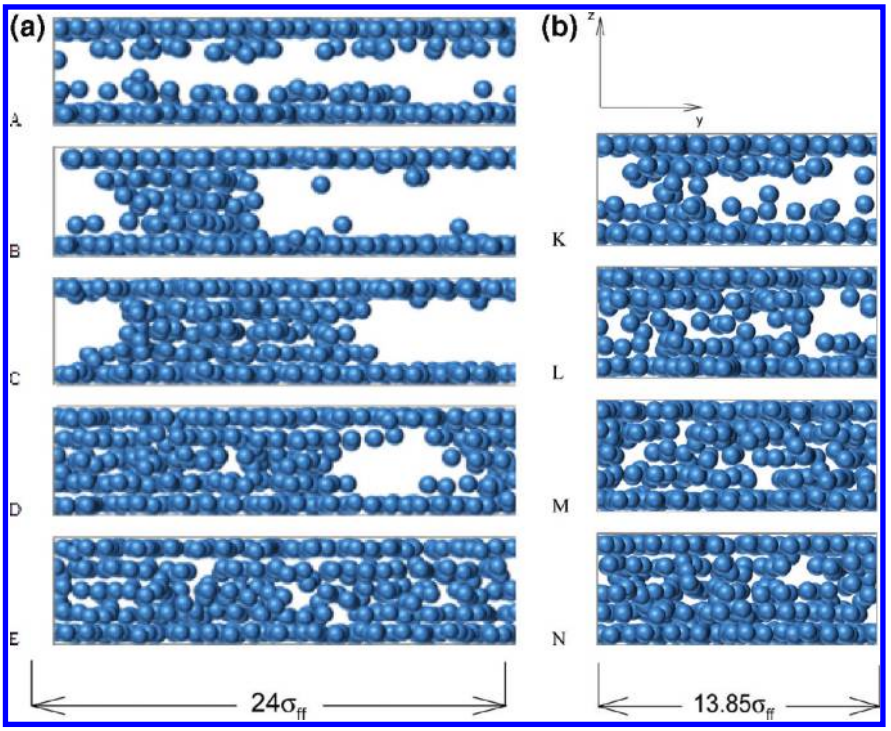

Figure 3. Snapshots for argon adsorption at 87.3 K in slit nanopores having: (a) rectangular surface and (b) square surface. The points A−E and K−N are indicated in Figure 2.

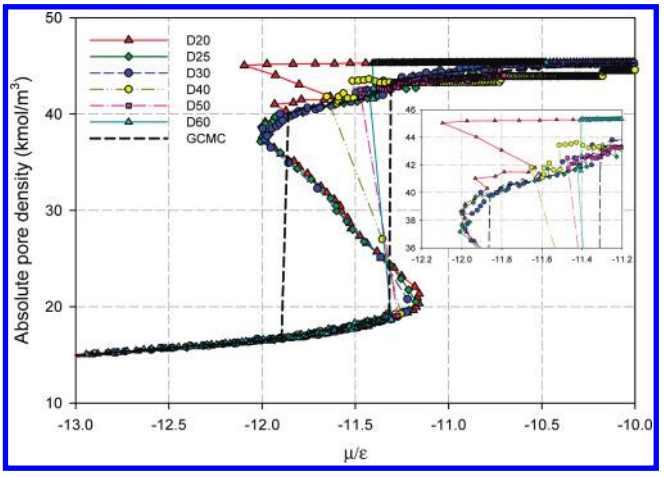

Figure 4. Effects of the size of the dosing volume on the meso-canonical isotherm of argon adsorption at 87.3 K in a 2 nm graphitic slit pore having square walls of dimensions of $10\sigma_{ff} \times 10\sigma_{ff}$.

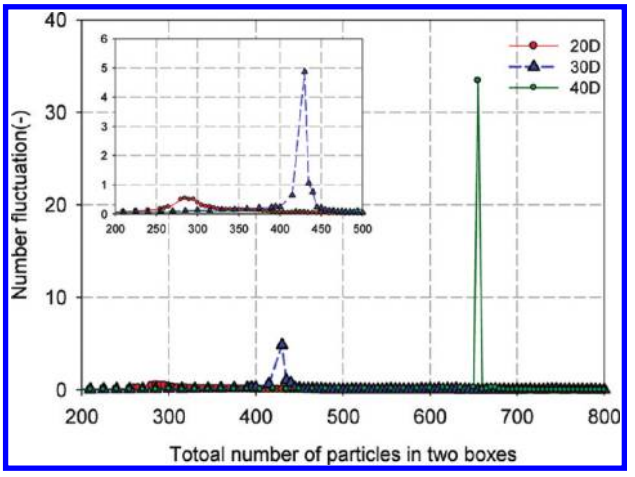

Figure 5. Effect of dosing size on the number fluctuation in the pore volume for argon adsorption at 87.3 K in a 2 nm graphitic slit pore having square walls of dimensions of $10\sigma_{ff} \times 10\sigma_{ff}$.

system jumps from a low density state to a high density state easier. The fluctuation in the pore volume is calculated by the following equation

$$F = \frac{f(N,N)}{\langle N \rangle} = \frac{\langle N^2 \rangle - \langle N \rangle^2}{\langle N \rangle} \qquad (4)$$

What is really interesting is that the level of the high density state at the end of the transition increases with the size of the dosing volume. For a dosing volume of D60, the high density state achieved at the end of the transition remains the same when the chemical potential is further increased. This density is very high and corresponds to the solid-like state of argon. The question is then why do we not observe this state when the sizes of the dosing volume of D25 and D30 are used? We explore this by reducing the dosing volume to D20, forcing the fluctuation to be substantially smaller (red circle symbols in Figure 5). The meso-canonical isotherm for this small size is also shown in Figure 4. At low densities, this isotherm is similar to those of D25 and D30. However, as the pore density has reached about 40 kmol/m^3, we observe the appearance of a second vdW loop which has not been reported in the literature. This loop basically represents the packing of argon particles in such a manner that it traces liquid-like states and solid-like states with intermediate states in between.

dx.doi.org/10.1021/jp202073r |J. Phys. Chem. B 2011, 115, 7862–7871

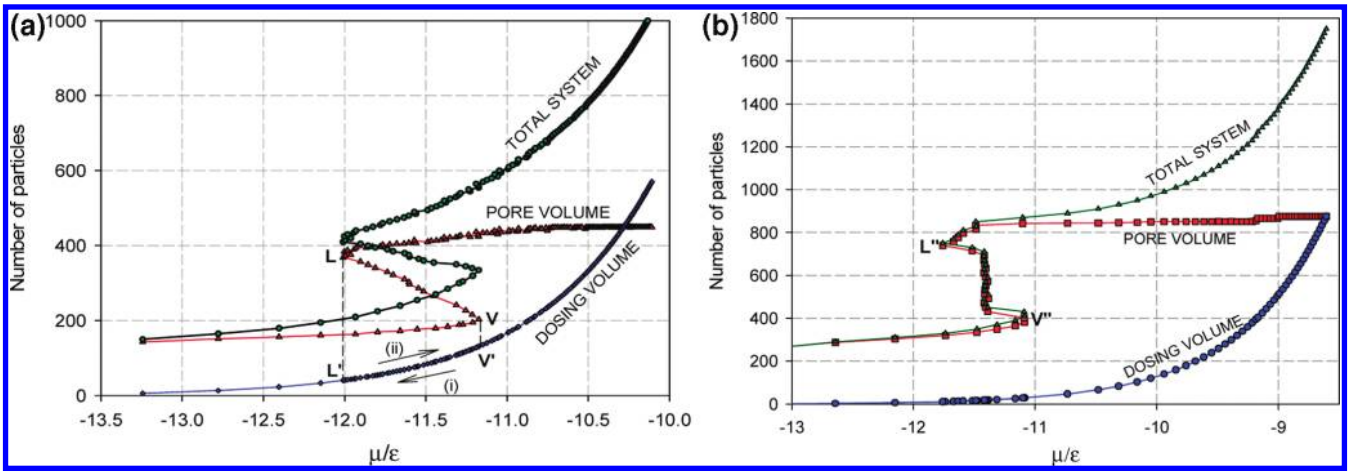

Figure 6. Plots of the equilibrium numbers of particle in the pore, in the dosing volume, and in the whole system as a function of chemical potential for argon adsorption at 87.3 K in 2 nm graphitic slit pore: (a) square walls of dimensions of $10\sigma_{ff} \times 10\sigma_{ff}$, dosing volume of D25; (b) rectangular walls of dimensions of $8\sigma_{ff} \times 24\sigma_{ff}$, dosing volume of D14.5.

Besides the additional vdW loop due to packing arrangement, the meso-canonical isotherms of D20, D25, and D30 are different from those corresponding to larger dosing volumes. This "intrinsic" unstable state of the meso-canonical isotherms (D20, D25, D30) is isolated because of the constraint imposed on the size of the dosing volume. However, we would like to stress that the intrinsic unstable state still depends on the pore geometry as we have discussed in Section 3.2 where the shape of the pore wall affects significantly the intermediate states. Since the combined two-volume system is canonical, the equilibrium is reached when the total Helmholtz free energy is a minimum

$$F_{pore} + F_{dosing} = \text{minimum}$$

Let N_{pore} be the number of particles in the pore cell. The minimization of the total Helmholtz free energy is equivalent to the first derivative of the above equation with respect to N_{pore} to be zero and its second derivative to be positive, i.e.

$$\frac{\partial}{\partial N_p}(F_{pore} + F_{dosing})\bigg|_{N,V,T} = 0 \tag{5}$$

$$\frac{\partial^2}{\partial N_p}(F_{pore} + F_{dosing})\bigg|_{N,V,T} > 0 \tag{6}$$

Since $dN_p = -dN_{dosing}$ because of the constant total number of particles, we have

$$\left(\frac{\partial F_{pore}}{\partial N_p}\right)_{N,T} = \left(\frac{\partial F_{dosing}}{\partial N_{dose}}\right)_{N,T} \tag{7}$$

and

$$\frac{1}{V_{pore}}\frac{\partial \mu_{pore}}{\partial \rho_{pore}} + \frac{1}{V_{dose}}\frac{\partial \mu_{dose}}{\partial \rho_{dose}} > 0 \tag{8}$$

where V_{pore} and V_{dose} are the sample and dosing volumes, respectively, and ρ_{pore} and ρ_{dose} are the pore density and the density of the dosing volume, respectively. Thus, the system can reach the minimum of the total Helmholtz free energy when the above inequality is satisfied. The change of the chemical potential of the dosing volume with its density is always positive, and as long as we choose the dosing volume small enough, we can have the above inequality satisfied even though the change of the chemical potential with the density in the pore is negative (unstable state). Therefore, the constraint on the size of the dosing volume to isolate the unstable branch of the meso-canonical isotherm is[11]

$$\frac{V_{dose}}{V} < \left|\frac{\partial \rho}{\partial \mu}\right| \Big/ \frac{\partial \rho_{dose}}{\partial \mu} \tag{9}$$

The dosing volumes of D20, D25, and D30 satisfy this inequality, while larger volumes of the dosing cell do not. This inequality also applies to the packing arrangement as well, and it is not difficult to prove that only the D20 dosing volume satisfies it.

We have seen how the meso-canonical isotherm behaves with the chemical potential (Figures 1, 2, and 4). To see how particles are distributed between the pore volume and the dosing volume, we plot the number of particles in these volumes as a function of the chemical potential, and we also plot them in terms of the total number of particles in the system. Such plots will show us how particles are distributed when more particles are added into the system.

We show the numbers of particles in the pore volume and the dosing volume as a function of chemical potential in Figure 6a for the system of argon adsorption in a 2 nm graphitic slit pore whose wall dimensions are $10\sigma_{ff} \times 10\sigma_{ff}$ and the dosing volume of D25. For chemical potentials less than the chemical potential at the vapor spinodal point (−11.3 in dimensionless units), the number of particles in the pore volume and the dosing volume increases. Beyond the vapor spinodal point (point V in Figure 6), we observe a continuous increase in the number of particles in the pore volume at the expense of the number of particles in the dosing volume; i.e., the number of particles in the dosing volume decreases, associated with a decrease in the chemical potential (arrow (i) in Figure 6). This will continue with the incremental dosing until the liquid spinodal point is reached (point L); after this point the number of particles in the two boxes increases. Thus, within the vdW loop, the number of particles in the dosing volume increases up to the vapor spinodal point, beyond which it decreases up to the liquid spinodal point, and then it increases

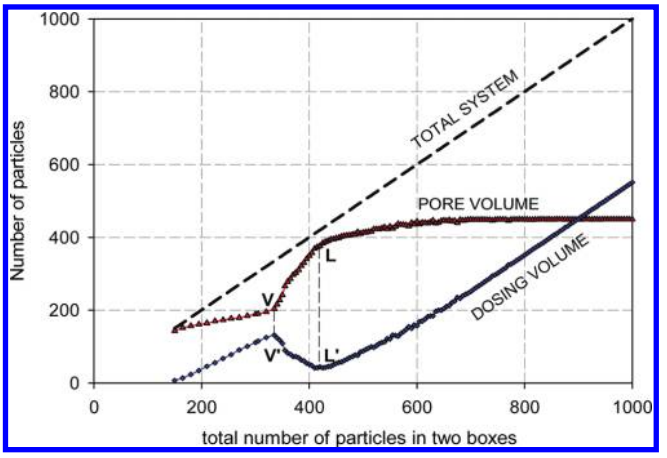

Figure 7. Plots of the equilibrium numbers of particles in the pore and in the D25 dosing volume as a function of total number of particles in two boxes for argon adsorption at 87.3 K in a 2 nm graphitic slit pore having square walls of dimensions of $10\sigma_{ff} \times 10\sigma_{ff}$.

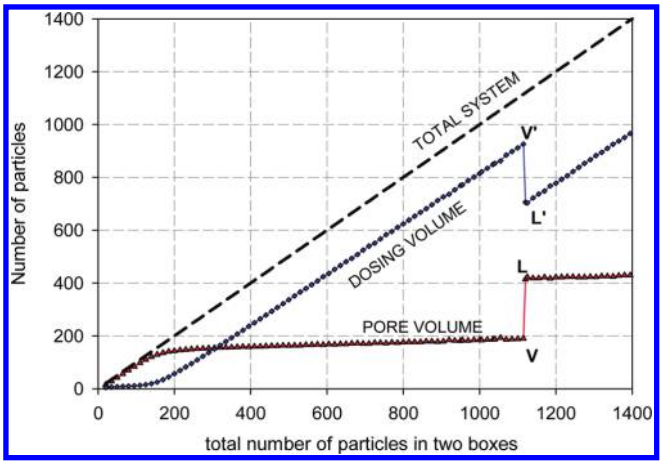

Figure 8. Number of particles in the pore cell and dosing cell D50 versus total number of particles in the system for argon adsorption at 87.3 K in a 2 nm graphitic slit pore having square walls of dimensions of $10\sigma_{ff} \times 10\sigma_{ff}$.

again. It is interesting to note that the increase in the number of particles in the pore with chemical potential is greater than the decrease in the number of particles in the dosing volume. This satisfies the inequality of eq 7.

We also show in Figure 6b the numbers of particles in the pore volume and the dosing volume as a function of chemical potential for the system of argon adsorption in 2 nm graphitic slit pore whose walls dimensions are $8\sigma_{ff} \times 24\sigma_{ff}$ and the dosing volume of D14.5. We observe that beyond the vapor spinodal (point "V" in Figure 6b) the number of particles in the pore volume increases while the chemical potential remains constant. As we have discussed in Section 3.2, this is due to the formation of a liquid bridge and the displacement of its two interfaces across the intermediate states to reduce the vapor bubble in the pore. After the liquid spinodal point "L" is reached, the number of particles in the pore volume and the dosing volume behave in the same way as those in the case of square walls. The formation of bridges and bubbles during adsorption and desorption in model pores was observed by Vishnyakov and Neimark[17] who noted the correspondence with the earlier thermodynamic model of Everett and Haynes.[18] To show the variation of the number of particles in the pore and the dosing volume with the total amount in the system, we plot them in Figure 7 as a function of the total number of particles. It is seen that the number of particles in the pore always increases with the total loading, while the number in the dosing volume increases up to the point which corresponds to the vapor spinodal point V in Figure 6 and then decreases up to the point which corresponds to the liquid spinodal point L, beyond which it increases again. This "starvation" effect is due to the increasing uptake of particles in the pore volume for it to achieve a state (unstable) which is neither rarefied nor dense. Once the pore is saturated, the number of particles in the pore reaches a plateau, while the number in the dosing volume increases linearly with the dose (pure physical filling of the dosing cell).

Let us now turn to the effects of the size of the dosing volume and study the change of the number of particles in the pore and dosing volumes as a function of total number of particles in the whole system. For the cases of smaller dosing volumes (D20, D25, and D30) along the unstable branch, the increase in the number of particles in the pore is greater than the decrease in the number of particles in the dosing volume, as typically shown in

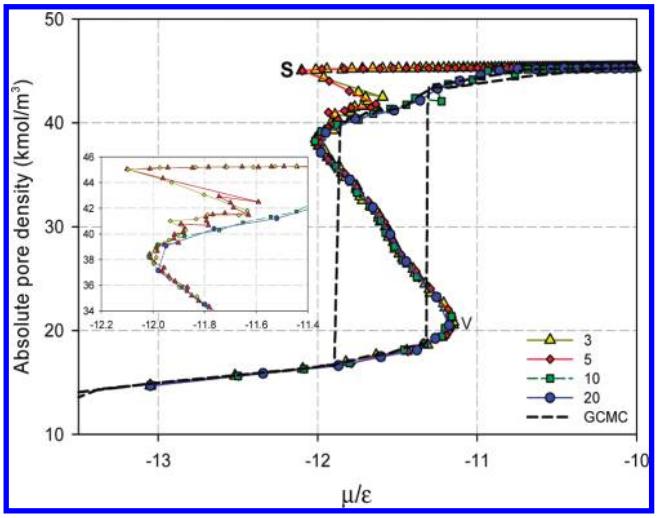

Figure 9. Effects of the dosing increment on the meso-canonical isotherm of argon adsorption in a 2 nm graphitic slit pore having square walls at 87.3 K with the D20 dosing volume.

Figure 7 with D25 dosing volume. However, in the cases of larger dosing volumes (D40, D50, and D60) the increase in the number of particles in the pore is similar to the decrease in the number of particles in the dosing volume, as shown in Figure 8 for the D50 dosing volume.

3.4. Effects of the Dosing Increment for Pores Having Square Walls. We investigate the effects of the dosing increment on the resolution of the unstable branch of the meso-canonical isotherm in the case of D20 dosing volume (Figure 9). A small dosing increment was added into the dosing volume for each equilibrium point to trace the vdW loop. When the dosing increment is ten particles or more we are able to trace the vdW loop of the vapor-like and liquid-like states. However, when we decrease the dosing increment to three or five particles we observe an additional vdW loop in the region of high density. This loop is due to a transition between liquid-like and solid-like states, when particles can rearrange to form a solid state. After the solid-like state has been reached (at the end of this loop, see point

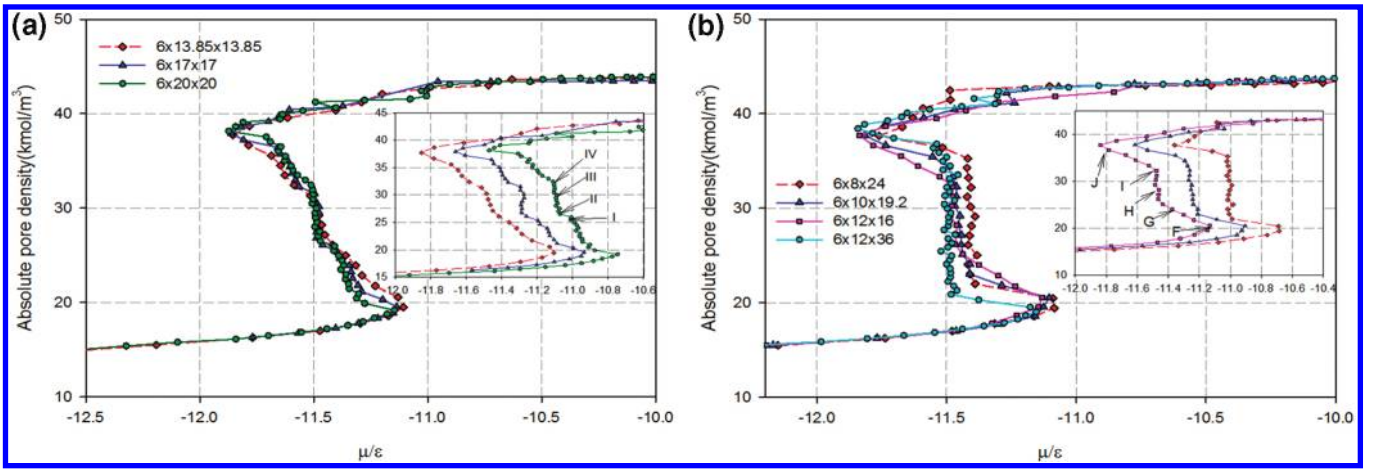

Figure 10. Effects of box size on the meso-canonical isotherm of argon adsorption in a $6\sigma_{ff}$ graphitic slit pore at 87.3 K with the ratio of two volumes equal to 67: (a) square surface and (b) rectangular surface (in the insets each curve was shifted horizontally by 0.2).

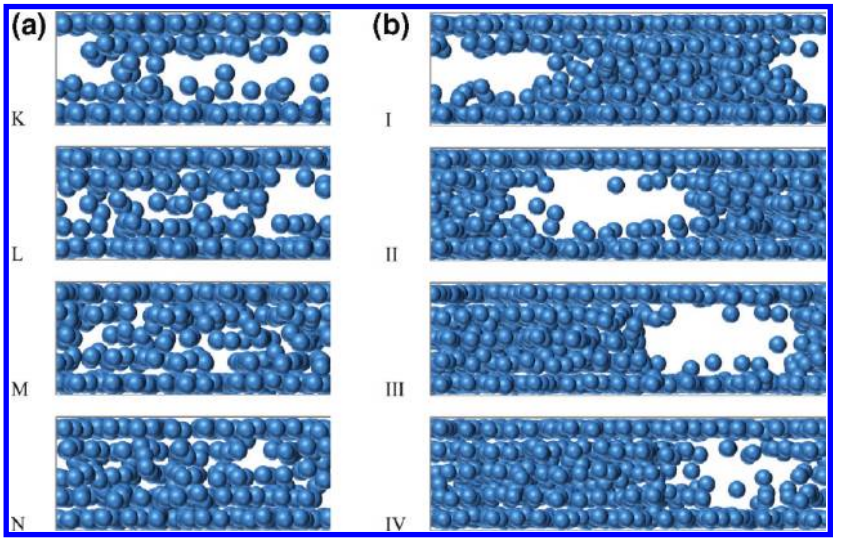

Figure 11. Snapshots for argon adsorption at 87.3 K in slit nanopores having square surface: (a) small surface 13.85 × 13.85 and (b) large surface 20 × 20. Points K−N are indicated in Figure 2, and points I−IV are indicated in Figure 10a.

S in Figure 9), this state remains unchanged no matter how much further the chemical potential is increased.

3.5. Effects of the Box Size. We have discussed in Section 3.2 that the meso-canonical isotherm depends on whether the pore wall is rectangular or square in shape. Now we investigate its dependence on the size of the pore volume and the dosing volume. Figure 10 shows the simulation results for argon adsorption at 87.3 K in a $6\sigma_{ff}$ graphitic slit pore. We keep the ratio of the dosing volume to the pore volume constant at 67 but vary the size and shape of these two boxes.

Figure 10a shows the simulation results for slit pores having square walls. For small linear dimensions of the wall, we observe a regular vdW with an S-shape. However, when the wall is larger we observe a vertical segment in the intermediate states, corresponding to the separation of the two phases. This separation occurs more easily in a larger box, and we support this with snapshots in Figure 11, where we show the configurations of the various points as marked in the meso-canonical isotherms of Figure 10a. The snapshots that show the clearest separation between the two phases correspond to a constant chemical potential.

Figure 10b shows the meso-canonical isotherms for rectangular walls with different dimensions. We observe a clear vertical segment in the intermediate states for a wall of dimensions $8\sigma_{ff} \times 24\sigma_{ff}$. However, the position of this vertical segment is different from that observed for the square wall (compare Figure 10a and 10b). When we increase the linear dimensions of the rectangular wall, the intermediate states move closer to those observed for the square wall due to the increase in the correlation length of the pore. We substantiate these observations with the snapshots as shown in Figure 12. As discussed earlier the vertical segment in the intermediate states results from the separation of the two phases with a clear formation of a liquid bridge and two vapor−liquid interfaces. Different points on the vertical segment correspond to different sizes of the liquid bridge.

3.6. Effects of Pore Size. Figure 13 shows the GCMC isotherms of argon adsorption in graphitic slit pores of 2, 3, and 4 nm width at 87.3 K, shown as dashed lines. The meso-canonical isotherms are also shown in the same figure as solid lines. The pore wall dimensions of the 2, 3, and 4 nm pores are 3.4 × 3.4, 4.5 × 4.5, and 6 × 6 nm, respectively, and the ratio of

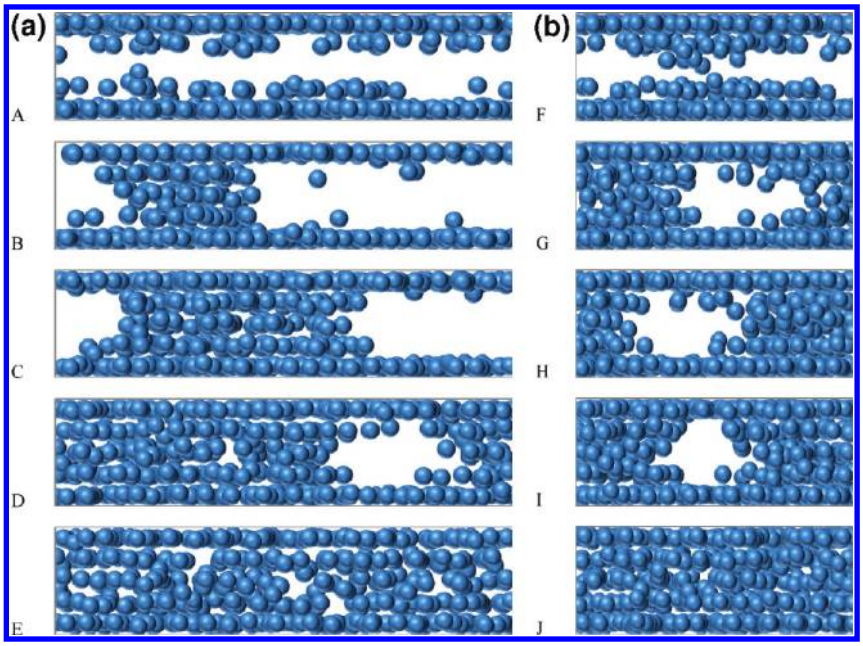

Figure 12. Snapshots for argon adsorption at 87.3 K in slit nanopores having rectangular surface: (a) 8 × 24 and (b) 12 × 16. The points A−F are indicated in Figure 2 and G−P are indicated in Figure 10b.

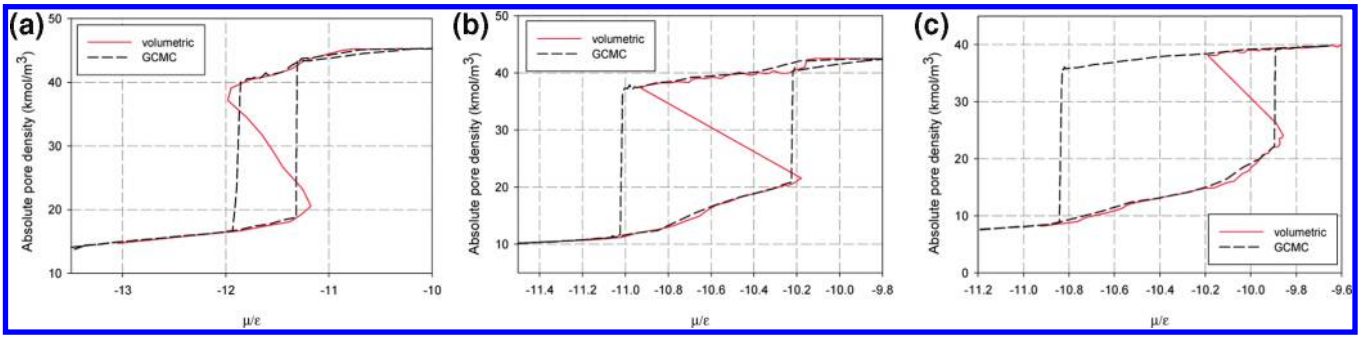

Figure 13. Effects of pore size on the meso-canonical isotherm of argon adsorption in graphitic slit pore for a specific choice of ratio between dosing volume and pore volume equal to 345: (a) 2 nm; (b) 3 nm; (c) 4 nm.

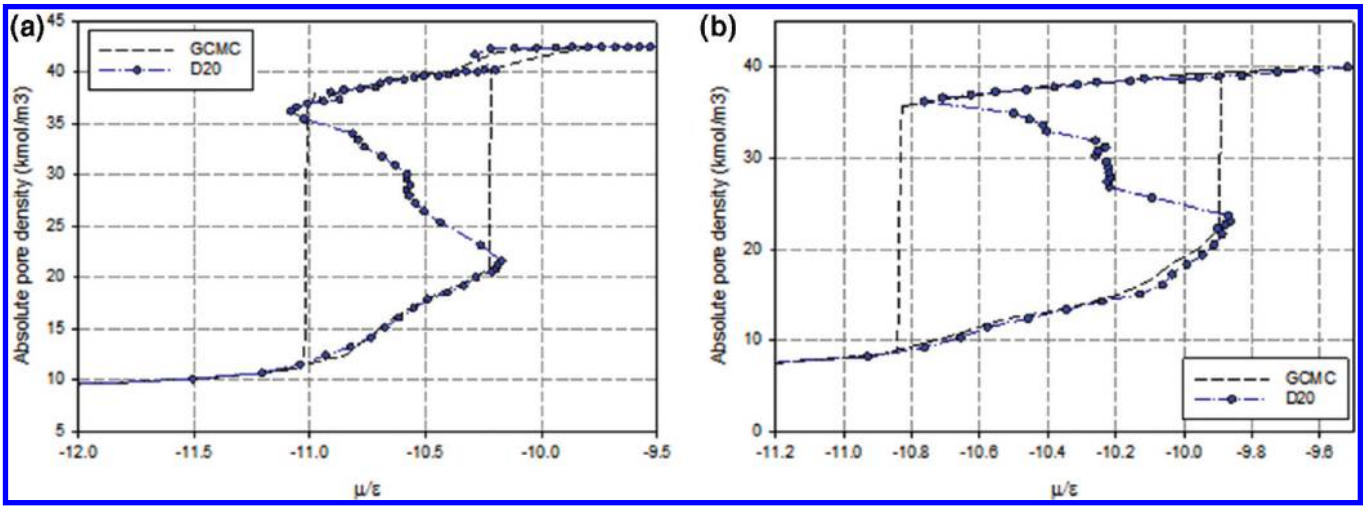

Figure 14. Plot of pore density (based on accessible volume) versus the chemical potential for argon adsorption in graphitic slit pore at 87.3 K: (a) 3 nm; (b) 4 nm.

dx.doi.org/10.1021/jp202073r |J. Phys. Chem. B 2011, 115, 7862–7871

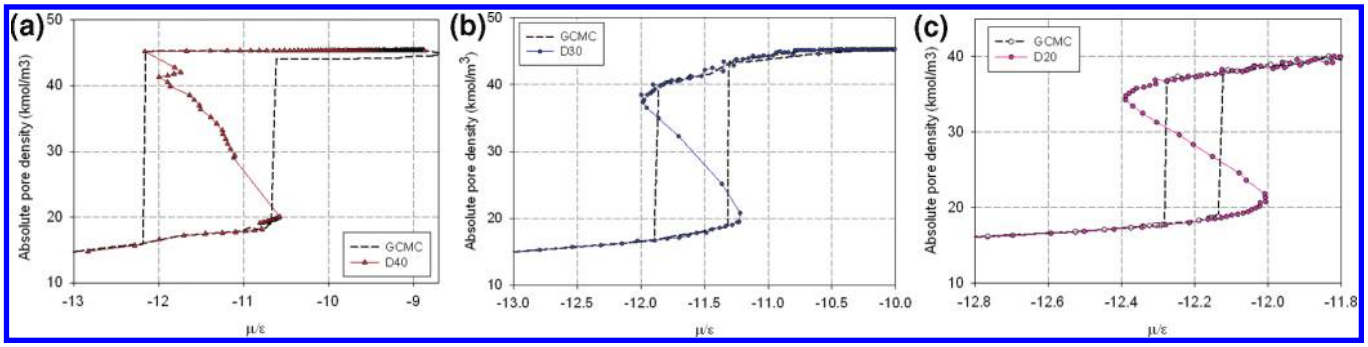

Figure 15. Effects of temperature on the meso-canonical isotherm of argon adsorption in 2 nm graphitic slit pore: (a) 77 K; (b) 87.3 K; (c) 100 K.

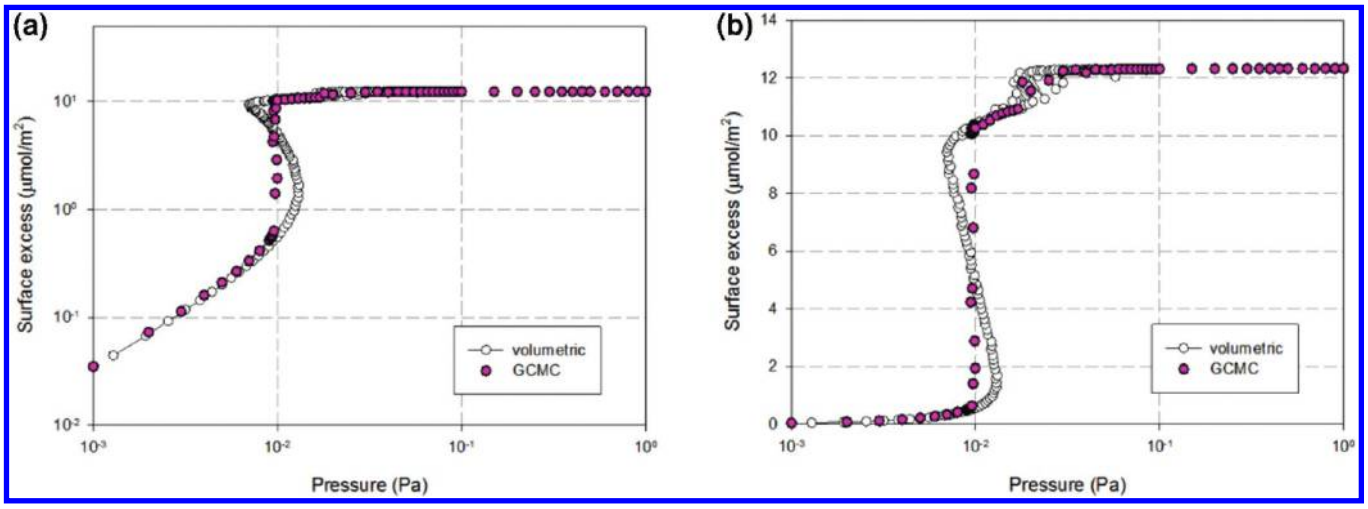

Figure 16. Plot of surface excess versus pressure for argon adsorption onto the graphitic surface at 55 K: (a) logarithm scale; (b) linear scale.

the dosing volume to the pore volume is 345. As the pore size is increased, the GCMC isotherm exhibits a wider hysteresis loop, as commonly observed in the literature.[4,19,20]

The meso-canonical isotherm traces the vdW loop, including stable, metastable, and unstable states for the 2 nm graphitic slit pore. On the other hand, due to large fluctuations in the slit pores of 3 and 4 nm width, the free energy barrier between the vapor-like and liquid-like phases is readily overcome, resulting in a jump in the density from the vapor-like state to the liquid-like state. Therefore, to trace the vdW loop, the ratio of dosing volume to the pore volume must be reduced from 345 to 131.7 and 55.55 for the 3 and 4 nm slit pores, respectively (Figure 14).

3.7. Effects of Temperature. In this section, we study the effects of temperature on argon adsorption in a 2 nm graphitic slit pore. Figure 15 shows the GCMC isotherms and the meso-canonical isotherms at 77, 87, and 100 K.

As temperature is increased, the hysteresis of the GCMC isotherms becomes smaller, and the vdW loop obtained with the meso-canonical method is smoother. At low temperatures the fluctuations in the pore are reduced, and therefore the system remains trapped in metastable states because of the complex energy landscape. As a result, the GCMC desorption branch extends down to the liquid spinodal point. This can be seen in Figure 15a. Moreover, we observe that as temperature is increased the difference between the point of spontaneous condensation and vapor-like spinodal as well as the difference between the point of spontaneous evaporation and liquid-like spinodal become more pronounced. Since the fluctuation in the pore increases with temperature, the dosing volume needed to trace the vdW loop should be smaller.

3.8. Study 2D-Transition for Adsorption onto the Graphite Surface. Finally, we apply the volumetric method for argon adsorption onto the graphite surface at 55 K. It is known that at this temperature adsorption shows a 2D-transition at very low pressure.[21,22] Figure 16 shows that the meso-canonical isotherm exhibits sigmoid behavior across the 2D-transition. This means that the unstable branch exists for both 3D- and 2D-transitions in the adsorbed phase.

4. CONCLUSION

The volumetric method allows one to construct the full phase diagram of a confined fluid in the form of a vdW loop, which includes stable, metastable, and unstable states. By studying adsorption of a simple atomistic fluid in slit nanopores having a square wall of small size, we observe a regular S-shaped vdW loop. However, when the wall area is increased we observe a vertical segment in the intermediate states, corresponding to the separation of the two phases. In contrast, there is a clear vertical segment in the intermediate states for a wall of dimensions $8\sigma_{ff} \times 24\sigma_{ff}$ as previously noted by Puibasset et al.[1] However, the position of this vertical segment is different from that observed for a square wall. When we increase the linear dimensions of the rectangular wall the intermediate states are similar to those for

the square wall. In the volumetric method the dosing volume can be used to control the level of fluctuation in the pore volume. The larger the dosing volume, the larger the fluctuation induced; hence, the unstable states of the system cannot be isolated; instead the system jumps from a low density state to a high density state. Therefore, to trace the vdW loop for large pores the ratio of dosing volume to the pore volume must be reduced. At low temperatures the fluctuations in the pore are reduced, and therefore the system remains trapped in metastable states because of the complex free energy landscape. As a result, the GCMC desorption branch extends down to the liquid spinodal point. Moreover, as temperature is increased, the difference between the point of spontaneous condensation and vapor-like spinodal as well as the difference between the point of spontaneous evaporation and liquid-like spinodal become more pronounced, and the dosing volume needed to trace the vdW loop is smaller because the fluctuation in the pore increases with temperature. The dosing increment also has a significant influence on the intermediate state. If it is chosen small enough, one can trace the vdW loop corresponding to liquid-like and solid-like states. The volumetric method shows that the unstable branch exists for both 3D- and 2D-transitions in the adsorbed phase.

AUTHOR INFORMATION

Corresponding Author

*Phone: +61-7-3365-4154. E-mail: d.d.do@uq.edu.au.

ACKNOWLEDGMENT

This work is supported by the Australian Research Council.

REFERENCES

(1) Puibasset, J.; Kierlik, E.; Tarjus, G. *J. Chem. Phys.* **2009**, *131* (12), 124123.
(2) Sing, K. S. W.; Everett, D. H.; Haul, R. A. W.; Moscou, L.; Pierotti, R. A.; Rouquerol, J.; Siemieniewska, T. *Pure Appl. Chem.* **1985**, *57* (4), 603.
(3) Jaroniec, M.; Gadkaree, K. P.; Choma, J. *Colloids Surf., A* **1995**, *118*, 203.
(4) Thommes, M.; Kohn, R.; Froba, M. *Appl. Surf. Sci.* **2002**, *196* (1−4), 239.
(5) Thommes, M.; Smarsly, B.; Groenewolt, M.; Ravikovitch, P. I.; Neimark, A. V. *Langmuir* **2006**, *22* (2), 756.
(6) Jagiello, J.; Betz, W. *Microporous Mesoporous Mater.* **2008**, *108* (1−3), 117.
(7) Jaroniec, M.; Kruk, M.; Li, Z. *Langmuir* **1999**, *15*, 1435.
(8) Morishige, K.; Fujii, H.; Kinukawa, D. *Langmuir* **1997**, *13* (No. 13), 3494.
(9) Morishige, K.; Tateishi, N.; Fukuma, S. *J. Phys. Chem. B* **2003**, *107* (22), 5177.
(10) Gardner, L.; Kruk, M.; Jaroniec, M. *J. Phys. Chem. B* **2001**, *105* (50), 12516.
(11) Neimark, A. V.; Vishnyakov, A. *Phys. Rev. E* **2000**, *62* (4), 4611.
(12) Neimark, A. V.; Vishnyakov, A. *J. Chem. Phys.* **2005**, *122* (23), 174508.
(13) Neimark, A. V.; Vishnyakov, A. *J. Phys. Chem. B* **2006**, *110* (19), 9403.
(14) Herrera, L.; Do, D. D.; Nicholson, D. *J. Colloid Interface Sci.* **2010**, *348* (2), 529.
(15) Frenkel, D.; Smit, B., *Understanding Molecular Simulation: From Algorithms to Applications*; Academic Press: San Diego, 1996.
(16) Jorge, M.; Seaton, N. A. *Mol. Phys.* **2002**, *100* (24), 3803.
(17) Vishnyakov, A.; Neimark, A. V. *J. Chem. Phys.* **2003**, *119* (18), 9755.
(18) Everett, D. H.; Haynes, J. M. *J. Colloid Interface Sci.* **1972**, *38* (1), 125.
(19) Thommes, M. In *Nanoporous Materials, Science & Engineering*; Lu, G., Zhao, X. S., Eds.; Imperial College Press: NJ, 2004; Vol. 4, p 317.
(20) Kaneko, K. *J. Membr. Sci.* **1994**, *96* (1−2), 59.
(21) Larher, Y.; Gilquin, B. *Phys. Rev. A* **1979**, *20* (4), 1599.
(22) Millot, F. *J. Phys. Lett.* **1979**, *40* (1), 9.